

# Microstructural and Mechanical Properties of In Situ WC-Fe/Fe Composites

Lisheng Zhong, Yinglin Yan, Vladimir E. Ovcharenko, Xiaolong Cai, Xi Zhang, and Yunhua Xu

(Submitted March 10, 2015; in revised form July 17, 2015; published online October 22, 2015)

**In this study, Fe matrix reinforced with column-shaped WC-Fe composite was designed and fabricated by a novel in situ method. The WC-Fe/Fe composite exhibited a similar structure to that of reinforced concrete. The microstructure, microhardness, impact toughness, and wear resistance of the composites were characterized using scanning electron microscopy, and x-ray diffraction, as well as microhardness, impact, and wear tests. Small amounts of graphite (G),  $\alpha$ -Fe, and WC were the predominant phases in the reinforcing bar of the composites. WC particulates improved the wear resistance of the composite, and the highest wear resistance was 96 times higher than that of gray cast iron under a load of 20 N with SiC abrasive particles. The wear resistance mechanism involved protection of the matrix behind the WC bundles by hard carbides. The excellent fracture toughness of the composite was mainly attributed to the disappearance of G flakes from the Fe matrix because of the in situ reaction, which reduced the split action to the matrix. The matrix absorbed a large amount of the crack propagation energy.**

**Keywords** fracture toughness, heat treatment, metal matrix composites (MMCs), wear

## 1. Introduction

Ceramic particulates are extensively used as reinforcement in metal matrix composites to improve their mechanical properties (Ref 1–3), including elastic modulus, strength, stiffness, wear resistance, and toughness (Ref 4, 5).

WC particles are an important class of reinforcement that present high hardness (22 GPa), a high melt temperature of 1720 °C, low coefficient of thermal expansion, moderate plasticity, and good wettability in ferrous melt (Ref 6). WC particle-reinforced steel or Fe matrix composites are desirable materials because of their low cost and wide availability of their reinforcements, which considerably reduces manufacturing costs and provides a good balance between price and mechanical properties (Ref 7–10). These materials exhibit isotropic properties with enhanced strength and stiffness compared with unreinforced materials. Ji et al. (Ref 11) prepared a composite metal containing WC particles and found satisfactory wear resistance. Kambakas et al. (Ref 12) prepared high-Cr white cast iron-WC particle-reinforced composites by a double casting technique that involves sand casting. The WC particles were directed to a specific location in the ingot and distributed uniformly in the working region of the material. The casting technique ensured chemical bonding between the high-Cr white cast iron and the particle-reinforced composite. Zhou et al. (Ref 13) prepared

a large area of crack-free Fe-based 20 wt.% WC coating using multitrack overlapping laser induction hybrid rapid cladding. The cast WC particles were dissolved almost completely and had worse wettability than that of Fe-based metal matrix. The precipitated carbides, such as  $M_{12}C$  and  $M_{23}C_6$  ( $M = Fe, W, Cr$ ), formed an intergranular network around the primary Fe-based phase enriched with W. Several other techniques have been employed to prepare WC-reinforced Fe-based composites, such as vacuum infiltration casting technique (Ref 14, 15), casting method (Ref 12), plasma melt injection (Ref 16), and plasma transferred arc method (Ref 17). These techniques are based on the addition of cast WC particles to matrix materials. In such cases, the reinforcing phase WC scale is limited by starting powder size, and the bonding strength of WC particles with the matrix is usually poor.

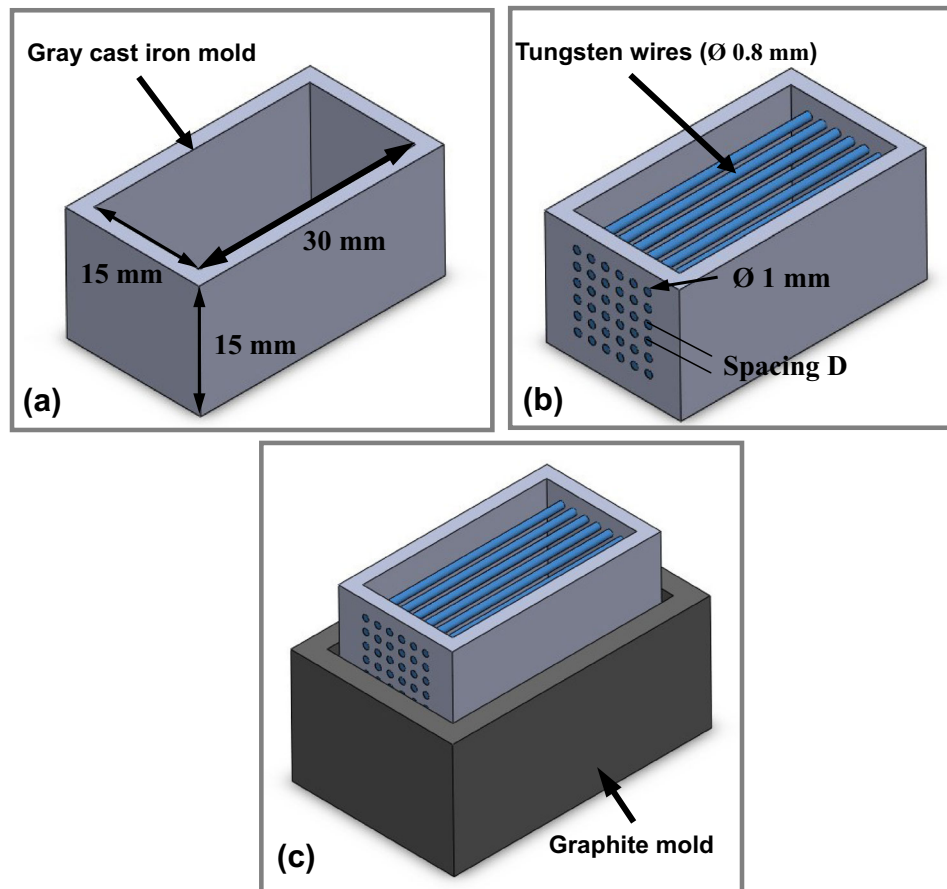
The suboptimal ductility of the matrix and its fracture behavior because of hard and brittle WC reinforcements must be addressed. WC particles block long-distance dislocation slips in the steel matrix and consequently reduce the in situ ductility of the matrix. Moreover, dislocations subject the matrix to high complex triaxial stress conditions, thereby increasing the tensile and yield strengths of the material. However, when a microcrack forms in the material under high triaxial stress, the matrix cannot blunt the crack efficiently, and the main crack rapidly branches out and propagates. This phenomenon is the primary reason for the low toughness of WC particle-reinforced steel matrix composites. Therefore, a material with optimal combination of toughness and stiffness must be developed to decrease the sensitivity of WC-reinforced steel or Fe matrix composites to cracks and flaws, as well as to increase static and dynamic properties.

Gray cast iron is a widely used engineering material that has low cost, suitable castability, good wear resistance, and toughness. In our work, gray cast iron was chosen as matrix of the composite and was employed as C source for in situ synthesis of WCs within the matrix. Flake graphite (G) causes gray cast iron to be more complex than other ferrous materials because stress is concentrated at the G tip (Ref 18). Most of the flake G in gray cast iron was consumed after in situ reaction,

**Lisheng Zhong, Yinglin Yan, Xiaolong Cai, Xi Zhang, and Yunhua Xu**, School of Materials Science & Engineering, Xi'an University of Technology, 5 Jinhua Road, Xi'an 710048, China; and **Vladimir E. Ovcharenko**, Institute of Strength Physics and Materials Science, Siberian Branch, Russian Academy of Sciences, Tomsk 634021, Russia. Contact e-mail: zhonglisheng1984@163.com.

**Table 1** Chemical composition of the starting materials (wt.%)

Materials	Chemical composition						
	C	Si	Mn	P	S	W	Fe
HT 300	3.45	1.40	1.47	0.116	0.100	...	Bal.
W 1	...	...	...	...	...	>99.95	...

**Fig. 1** 3D image of (a) the gray cast iron mold, (b) the preform, and (c) the graphite mold used in the experiment

and high hardness WC particles were generated, which improved the wear resistance and toughness of the material.

In this study, Fe matrix reinforced by a high-volume fraction column-shaped WC-Fe composite was designed and fabricated by a novel in situ method. The obtained WC-Fe/Fe composite exhibited similar structure to that of reinforced concrete. A sufficiently non-deformed matrix between the reinforcements absorbed the fracture energy, prevented crack formation, and efficiently improved the toughness, especially the crack propagation resistance, of the WC-reinforced steel matrix composite. The arrangement of the WC-Fe/Fe composite demonstrated high particle volume fractions in some areas of the bulk material and other unreinforced areas between composites, which can efficiently blunt cracks. Thus, reinforcements not only sufficiently strengthened the matrix but also improved the toughness of the material. The microstructure, microhardness, flexure strength, and wear resistance of the WC-Fe/Fe composite were investigated by scanning electron microscopy (SEM) and x-ray diffraction (XRD), as well as microhardness, impact, and wear tests.

## 2. Experimental Procedures

### 2.1 Materials

The starting materials were gray cast iron (HT300) and W wire ( $\text{Ø} = 0.8 \text{ mm}$ ) with 99.95% purity (W1). These materials were employed as C and W sources, respectively, for in situ synthesis of WCs within the iron matrix. The chemical composition of gray cast iron and W wire (in wt.%) is listed in Table 1.

### 2.2 Experimental Procedure

The WC-Fe/Fe composite was prepared according to the following procedure. The gray cast iron mold was fabricated into a rectangular shape, as shown in Fig. 1(a). A number of holes were inversely drilled (diameter = 1.0 mm) on both sides, with different target distances between the holes. The W wires were passed through the holes on both sides and then firmly fixed to the mold (Fig. 1b). The iron mold was then inserted into the G mold (Fig. 1c). All dimensions of the mold are indicated in Fig. 1.

Molten gray cast iron was produced in a medium-frequency induction furnace and poured into the mold at 1430 °C. The specimen was immediately covered with quartz sand to avoid crack generation, and was cooled down to room temperature. The as-cast samples were subjected to heat treatment in a horizontal tube furnace (model GSL1400; Hefei Kejing Materials Technology Co., Ltd., Anhui China) with a modest flow of Ar and naturally cooled down to room temperature.

To determine the heat treatment temperature of the as-cast sample, differential scanning calorimetry (DSC)/thermogravimetric analysis was performed on a SDT Q600 (TA Instruments, New Castle, DE, USA) for a cylindrical sample having a diameter of 2 mm and height of 2.6 mm prepared from gray cast iron and W wire. The sample was heated at 10 °C/min up to a maximum temperature of 1400 °C with a 150 ml/min flow rate of Ar gas and cooled down to room temperature.

### 2.3 Characterization

The specimen was polished with diamond paste and etched with a 4% Nital solution. Afterward, the microstructure of the specimen was examined using a JSM-6700F scanning electron microscope (SEM; JEOL, Tokyo, Japan). XRD data were recorded on an XRD-7000 (Shimadzu Limited, Tokyo, Japan) with monochromatic Cu  $K_{\alpha}$  radiation at 40 kV and 40 mA in the  $2\theta$  range of 10°-90°.

Microhardness of the specimens was measured according to ASTM: E384-11e1, which is the standard test method for Vickers hardness of metallic materials. Macrohardness of samples was measured according to ASTM: E18-12, which is the standard test method for Rockwell hardness of metallic materials.

### 2.4 Abrasive Wear Test

The bulk composites specimen was cut to a size of 6 mm (diameter) × 25 mm for the abrasive wear test. The test was carried out on an ML-100 wear test machine (Zhangjiakou Xuan Ke Testing Machine Manufacturing Co., Ltd., China). The abrasive wear resistance was tested according to JB/T 7506-1994, which is the mechanical industry standard of China. Abrasion tests were carried out using a pin-on-disk apparatus. The flat cylinder was loaded through a vertical specimen holder against a horizontal rotating disk (25 rpm) covered with SiC, Al<sub>2</sub>O<sub>3</sub>, or SiO<sub>2</sub> abrasive paper of which the particle size was 600 mesh, with different loads. The specimen was moved over the abrasive paper in a spiral motion such that fresh abrasive was always encountered. The weight loss of the pin was measured in an analytical balance with a 0.0001 g precision. The weight loss was converted to volume loss values.

The relative wear resistance,  $\beta$ , was used to evaluate the abrasive wear properties of the WC-Fe/Fe composites. This can be obtained by first computing the abrasive volume using the equation

$$\Delta V = \frac{\Delta m}{\rho}, \quad (\text{Eq 1})$$

where  $\Delta V$  is the abrasive volume,  $\Delta m$  is the weight loss after abrasion, and  $\rho$  is the density of the test material. The relative wear resistance is defined as

$$\beta = \frac{\Delta V_r}{\Delta V_c}, \quad (\text{Eq 2})$$

where  $\beta$  is the relative wear resistance,  $\Delta V_r$  is the abrasive volume of the gray cast iron reference sample, and  $\Delta V_c$  is the abrasive volume of the WC-Fe/Fe composites. The wear test was repeated at least three times for each sample.

### 2.5 Impact Strength and Fracture Toughness Test

The Charpy impact test was applied to measure the impact toughness of the gray cast iron and the WC-Fe/Fe composites at 25 °C using JB-W impact test machine (Jinan Puye Electrical and Mechanical Technology Co., Ltd., China). The impact toughness specimens with dimensions of 10 mm × 10 mm × 55 mm in dimensions were prepared according to ASTM: E23-82. The G flakes acted as crack starter in the specimen, and thus, an extra notch was not machined on the specimen. The test was repeated at least three times for each specimen, and the average of the test results was used in the evaluation.

Vickers microindentation fracture toughness tests were carried out with an HVS-1000 microhardness tester employing the ASTM: E384 standard. For the fracture toughness values, Vickers diagonals ( $l$ ) and crack lengths ( $g$ ) were measured in an Olympus GX51 microscope under 50× and 100× magnifications using the measurement thickness tool of the MSQ Plus Software. The Palmqvist crack model proposed by Laugier (Ref 19) was used to determine the fracture toughness of the column-shaped WC-Fe composites.

$$K_{Ic} = k^p \left(\frac{g}{l}\right)^{-\frac{1}{2}} \left(\frac{E}{H}\right)^{\frac{3}{2}} \frac{P}{c^{\frac{3}{2}}}, \quad (\text{Eq 3})$$

where  $K_{Ic}$  is the fracture toughness,  $E$  is Young's modulus,  $H$  is microhardness,  $P$  is applied load,  $g$  is microcrack length,  $l$  is half diagonal length of the microindentation,  $\varphi$  is constraint factor ( $\varphi \approx 3$ ),  $k_p$  is 0.015, and  $c$  is the total crack length.

### 2.6 Flexure Strength Test

The bulk composite specimens were cut to 20 mm × 4 mm × 3 mm for the flexure strength test according to GB/T232-2010, which is the national standard of China. The test was carried out on a DEW-30 universal material testing machine (Xiamen Deyi Testing Machine Co., Ltd., China). The flexure strength,  $\sigma_b$ , is defined as

$$\sigma_b = \frac{3PL}{2bh^2}, \quad (\text{Eq 4})$$

where  $P$  is the maximum bending loads,  $b$  is the width of the sample,  $h$  is the height of the sample, and  $L$  is the effective length.

All the specimens were taken out and cut by a numerically controlled wire-cut EDM machine (Suzhou Nutac Electro Mechanic Co., Ltd., China).

## 3. Results and Discussion

### 3.1 DSC Analysis and Heat Treatment Temperature

The thermal behaviors of specimens manufactured from gray cast iron and W wire are shown in Fig. 2. In the DSC curve, two endothermic peaks with relatively higher intensities centered at 773 and 1160 °C were found. One endothermic

peak with relatively lower intensity is centered at 1293 °C, and one exothermic peak is centered at 1340 °C.

The endothermic peak at 773 °C can be assigned to an allotropic change  $\alpha\text{-Fe} \rightarrow \gamma\text{-Fe}$  (Ref 20), and the endothermic peak at 1160 °C can be due to the ternary eutectic transformation  $L \rightarrow \gamma\text{-Fe} + G + \text{WC}$  or  $L \rightarrow \gamma\text{-Fe} + G + (\text{Fe,W})_6\text{C}$  (Ref 21). The endothermic peak at 1293 °C can be assigned to WC formation by the reaction  $C + W \rightarrow \text{WC}$  between C from the Fe matrix and W from the wire (Ref 22). The exothermic peak at 1340 °C is attributed to the formation of primary carbide.

The eutectic temperature of the Fe-C-W system was 1085 °C according to the liquidus projection (Fig. 2, inset). The chemical change at this temperature is as follows:



Thus, WC cannot be produced until the heat treatment temperature is above 1085 °C. The reaction that occurs near the ternary eutectic transformation is conducive to the precipitation of G and maintenance of matrix consistency. Based on the DSC curve and liquidus projection of the Fe-C-W system, 1160 °C was selected as the optimum temperature for further heat treatment of the as-cast samples.

### 3.2 Microstructure

Figure 3 shows an SEM micrograph of the WC-Fe/Fe composite. After heat treatment at 1160 °C for 12 h, the

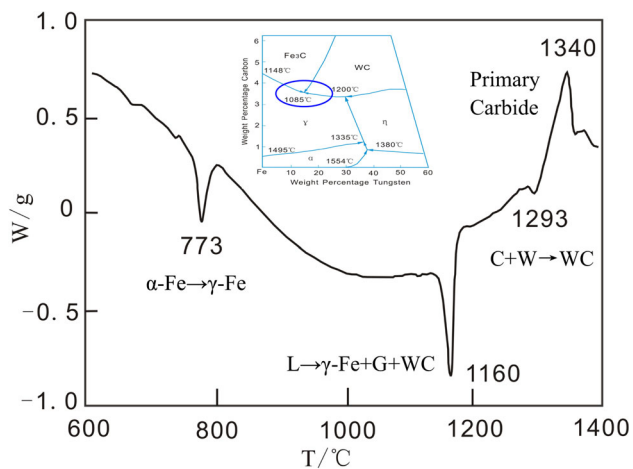


**Fig. 2** DSC curve of the specimen prepared from tungsten and cast iron (inset: liquidus projection of the Fe-C-W system)

column-shaped reinforcement composed of WC particles replaces the W wire in situ (Fig. 3a). The diameter of the column-shaped reinforcement was 1.0-1.2 mm, and the center-to-center spacing between WC particulate bundles was approximately 2.5 mm (Fig. 3a). The quantity and size of G in the Fe matrix decreased substantially because of the in situ reaction. Figure 3(b) and (c) shows that the column-shaped reinforcement is a type of particle-reinforced Fe matrix composite, of which the volume fraction exceeds 90%. Moreover, the size of the carbide particles varies between 10 and 15  $\mu\text{m}$ .

XRD analysis was performed to confirm the reinforcement phases present in the composite. Figure 4 shows that WC was the predominant phase in the reinforcing bar of the composite. Small amounts of G,  $\alpha\text{-Fe}$ , and WC were detected in the composition. WC was produced by the reaction between W and C at the eutectic temperature. The matrix of the composites was made of  $\alpha\text{-Fe}$ , and a small amount of G was separated out by a few unreacted C atoms in the matrix. Therefore, the column-shaped reinforcement consisted of high-volume fraction WC particle-reinforced Fe matrix composite, i.e., WC bundles.

### 3.3 Microhardness

Table 2 shows the microhardness values of the WC-Fe/Fe composites. The average microhardness of the WC bundles was 2385  $\text{HV}_{0.05}$ , whereas that of the  $\alpha\text{-Fe}$  matrix between the WC bundles was 360  $\text{HV}_{0.05}$ . The microhardness of the WC bundles was much higher than that of the  $\alpha\text{-Fe}$  matrix. Thus, the contribution of the WC bundles to the abrasive wear resistance of the composite should be larger than that of the  $\alpha\text{-Fe}$  matrix. The support and protection provided by the  $\alpha\text{-Fe}$  matrix to the WC bundles are also crucial. WC bundles cannot be extracted or dropped from the  $\alpha\text{-Fe}$  matrix if the composite hardness is appropriate under the wear conditions. Three types of abrasive particles, namely,  $\text{Al}_2\text{O}_3$ , SiC, and  $\text{SiO}_2$ , were selected to evaluate the wear resistance of the WC-Fe/Fe composites. The hardness of  $\text{Al}_2\text{O}_3$  was similar to that of WC-Fe, and the hardnesses of silicon carbide SiC and silicon oxide  $\text{SiO}_2$  were higher and lower, respectively, than that of WC-Fe.

### 3.4 Abrasive Wear Resistance

The relative wear resistance of the WC-Fe/Fe composite as a function of applied loads is shown in Fig. 5. The specimen exhibits a much higher wear resistance than the gray cast iron. The relative wear resistance of WC-Fe/Fe composite increased with the load regardless of the type of abrasive used, and the

**Table 2** Microhardness values of the WC-Fe composites and matrix and MOHS hardness values of abrasive particles

Hardness	Matrix ( $\text{HV}_{0.05}$ )	WC-Fe composites ( $\text{HV}_{0.05}$ )	Abrasive particles (MOHS)		
			$\text{SiO}_2$	$\text{Al}_2\text{O}_3$	SiC
1	364	2362	6-7 (a)	8.8 (a)	9.5 (a)
2	351	2350			
3	368	2349			
4	355	2369			
5	362	2395			
Average	360	2385	6-7 (a)	8.8 (a)	9.5 (a)

(a) Data from the literature



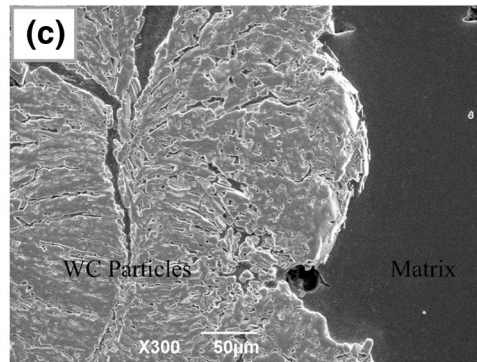
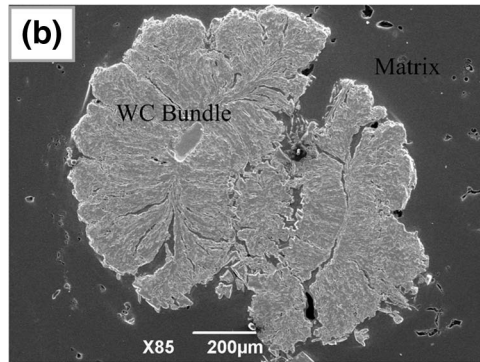
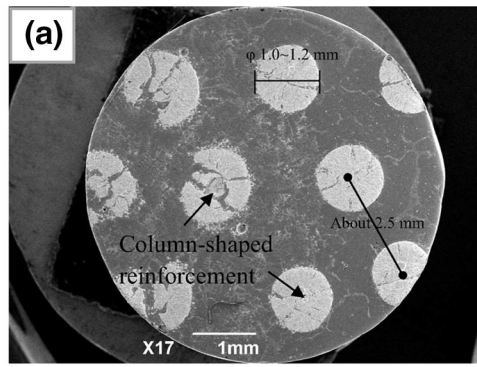


**Fig. 3** SEM of the WC-Fe/Fe composites at 1160 °C for 12 h: (a) whole; (b) part; (c) the particles

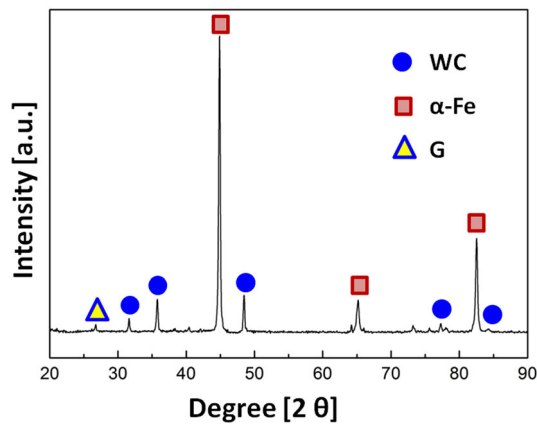


**Fig. 4** XRD analysis of in situ WC-Fe/Fe composite at 1160 °C for 12 h

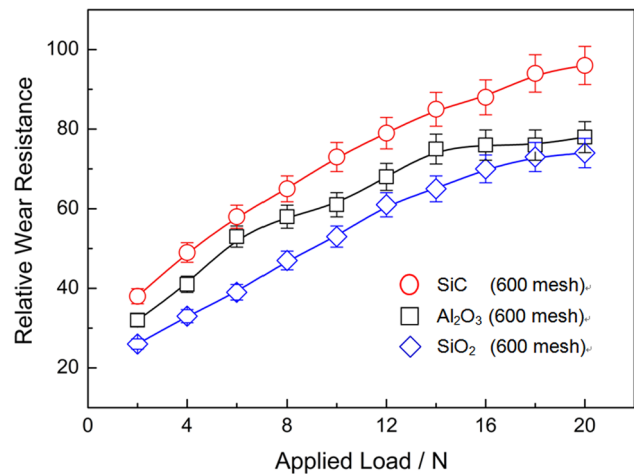


**Fig. 5** The relative wear resistance of WC-Fe/Fe composite with different abrasive particles under different loads

change trend is consistent with that of homogeneous materials. The WC-Fe/Fe composite with SiC abrasive particles exhibited the best wear resistance among the specimens surveyed, and the wear resistance values of the WC-Fe/Fe composites were 38 and 96 times higher than that of the gray cast iron under loads of 2 and 20 N, respectively. The wear resistance of the composite with SiO<sub>2</sub> abrasive particles was 26 and 74 times higher than that of the gray cast iron under loads of 2 and 20 N, respectively. The wear resistance observed with Al<sub>2</sub>O<sub>3</sub> abrasive particles was between those of composites with SiC and SiO<sub>2</sub>. The WC-Fe/Fe composites display excellent abrasion resistance under hard abrasive wear. The substantial increase in wear resistance of the WC-Fe/Fe composites is attributed to the WC bundles produced in situ.

The wear morphology of the composite with Al<sub>2</sub>O<sub>3</sub> abrasives under a 20 N load is shown in Fig. 6. The WC bundles influence the working direction of the abrasives. For single WC bundles, severe wear of the matrix and WC bundles was observed in the abrasive motor direction. Obvious cutting and plowing can be observed in Fig. 6(a). By contrast, the matrix and WC bundles in the opposite direction were not significantly damaged, and the matrix behind the WC bundles was protected. The angle ( $\alpha$  in Fig. 6) between the cutting marks and interface influences the interaction of abrasive particles and WC bundles. When  $45^\circ < \alpha < 90^\circ$ , the abrasive particles and WC bundles collided head-on. The WC particles

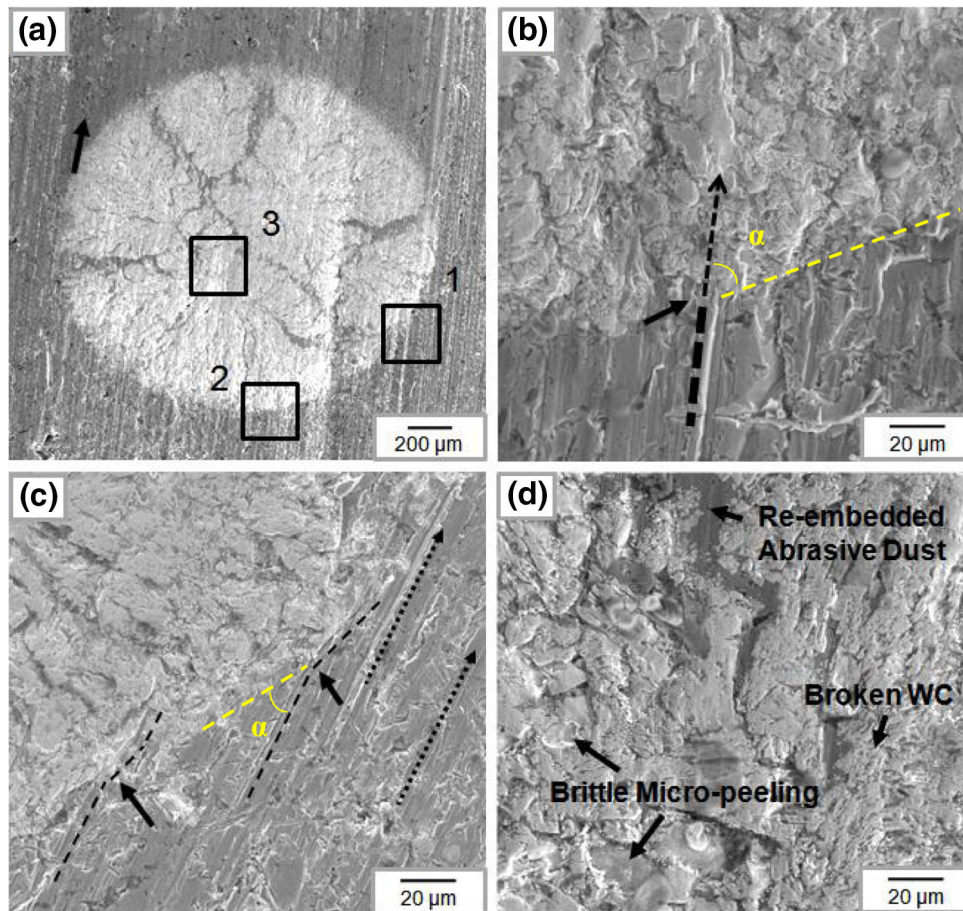


**Fig. 6** Wear morphologies of the composites under 20 N load with  $\text{Al}_2\text{O}_3$  abrasive: (a) WC-Fe bundles; (b), (c) interface between WC bundles and the gray cast iron matrix; (d) within the WC-Fe bundles

**Table 3** Mechanics properties of the WC-Fe/Fe composite and gray cast iron

	Flexure strength, MPa	Fracture toughness ( $K_{IC}$ ), $\text{MPa m}^{0.5}$	Elongation, %	Impact toughness, $\text{J/cm}^2$	Hardness, HRC
WC-Fe/Fe composite	739	26.2	4.5	10.4	48
Gray cast iron (HT300)	648	18.6	3.8	8.2	26

in the bundle were broken because of brittle collisions between  $\text{Al}_2\text{O}_3$  and WC. The cutting marks in the WC bundles became narrow and shallow (Fig. 6b). By contrast, when the cutting marks encountered WC bundles at  $\alpha < 45^\circ$ , some of the furrows were directed straight toward the center of the WC bundles but the width and depth of the furrows were low. The other direction of the furrows changed toward the matrix (Fig. 6c).

Figure 6(d) shows the wear appearance of the WC bundles. Some WC particles in the WC bundles exhibited brittle micropeeling because of interactions with abrasive particles. A number of the WC particles were broken under the load, with some of these broken particles re-embedded into the matrix, thereby functioning as reinforcing particles.

Wear properties are affected not only by the hardness of the composite ( $H_m$ ) and abrasive ( $H_a$ ) materials but also by the ratio of  $H_a/H_m$ . According to Richardson's theory (Ref 23, 24), material abrasion is very low when  $H_a/H_m \leq 0.7$ -1.1. The hardness values of the WC-Fe bundle and  $\text{Al}_2\text{O}_3$  abrasive were approximately 2385 and 1800 HV, respectively, whereas that of

the matrix was 360 HV. Thus,  $H_{\text{Al}_2\text{O}_3}/H_{\text{WC-Fe}} = 1800/2385 = 0.75 < 1.1$ , and  $H_{\text{Al}_2\text{O}_3}/H_m = 1800/360 = 5 > 1.1$ . In the WC-Fe/Fe composite, the matrix experienced high abrasion conditions, whereas the WC-Fe bundle experienced relatively low abrasion conditions.

In summary, the main abrasive wear mechanism of the novel WC-Fe/Fe composite is protection of the matrix behind WC bundles by the hard carbide. Microcutting and microplowing are the main causes of wear in the matrix. By contrast, broken WC, brittle micropeeling, and broken particles re-embedded in the matrix are the main wear mechanisms in the WC bundles.

### 3.5 Mechanical Properties

Table 3 lists the mechanical properties of the novel composite and gray cast iron. The flexural strength of the WC-Fe/Fe composite was approximately 739.16 MPa, which was higher than that of the gray cast iron (647.91 MPa). The fracture toughness ( $K_{IC}$ ) and impact toughness ( $\alpha_k$ ) of the composites were 26.2  $\text{MPa m}^{0.5}$  and 10.4  $\text{J/cm}^{-2}$ , respectively, which were



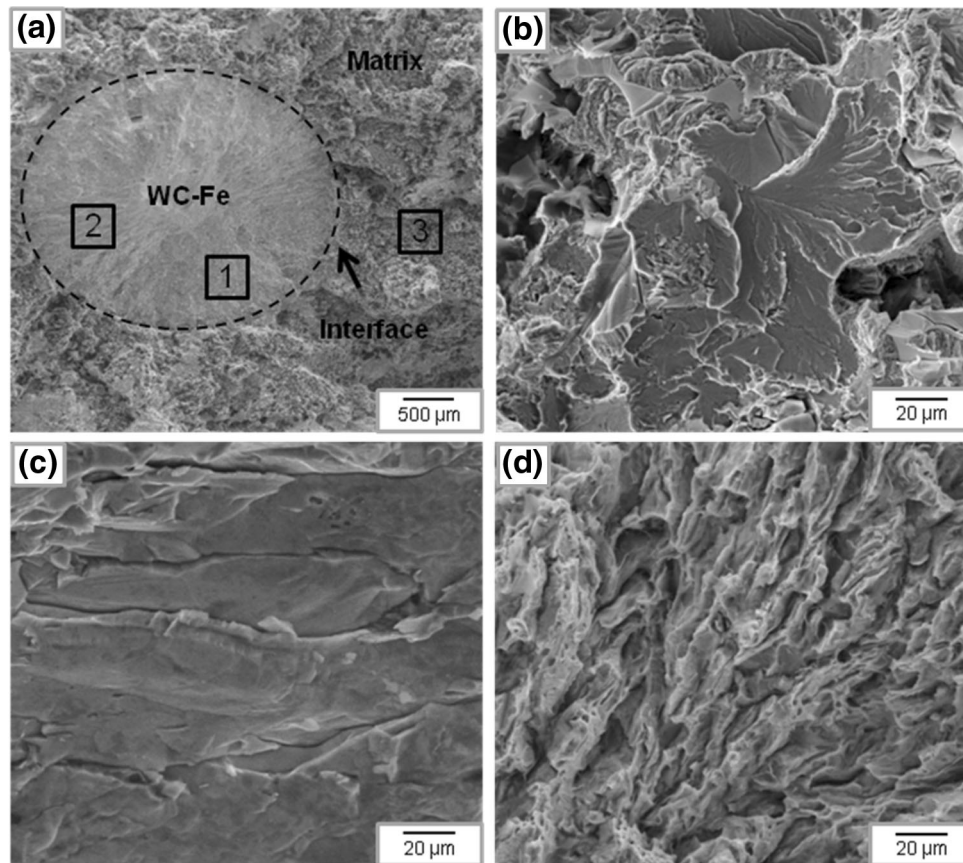


**Fig. 7** Fracture morphology of the WC-Fe/Fe composite: (a) whole reinforced zone; (b) sector cleavage in the WC-Fe bundle; (c) rock candy-shaped fracture in the WC-Fe bundle; (d) numerous dimples in the Fe matrix

also higher than that of the gray cast iron. The elongations of the composite and gray cast iron were 4.5% and 3.8%, respectively. The disappearance of G flakes caused by the in situ reaction between W and C was the main reason for the enhanced composite mechanical properties. The formation of large areas of homogeneous matrix with low C content absorbs the crack propagation energy and improves the mechanical properties of the composites.

Magnified SEM micrographs of the composites after the transverse tests are shown in Fig. 7 to elucidate the fracture mechanism. Cleavage fractures, which are a type of transgranular fracture, are the main fracture characteristic of the WC bundles. These fractures are caused by the high volume fraction of carbides in the bundles. Numerous dimples are found in the Fe matrix because of the disappearance of G flakes, and ductile fractures are the main fracture characteristic of this material. Cleavage fracture of the metal hardly occurs along the crystal face, so cleavage cracks cross several parallel cleavage planes and form cleavage steps. This process is the formation principle of the sector cleavage. Strip particles fill the matrix, and rock candy-shaped fractures, which are another type of intergranular fracture, can be observed. Rock candy-shaped fractures could hinder considerable improvement of the flexural strength of a composite.

The primary causes of the enhanced toughness of the WC-Fe/Fe composite are as follows:

- (1) G flakes disappear from the Fe matrix because of the in situ reaction, which reduces the split action to the matrix.

- (2) Crack initiation and propagation first occur in WC bundles because of their brittleness. When the crack grows into the matrix, the crack propagation energy is absorbed by the matrix. The toughness of the composite is improved by inhibiting crack propagation.

#### 4. Conclusions

- (1) Based on the DSC curve and liquidus projection of the Fe-C-W system, 1160 °C was selected as the optimum temperature for heat treatment of the as-cast samples. After heat treatment at 1160 °C for 12 h, the column-shaped reinforcement replaced the W wire in situ. The diameter of the column-shaped reinforcement ranged from 1.0 to 1.2 mm, and the center-to-center spacing between WC particulate bundles was approximately 2.5 mm. The average microhardness of WC bundles was 2385 HV<sub>0.05</sub>, whereas that of the  $\alpha$ -Fe matrix between WC bundles was 360 HV<sub>0.05</sub>.
- (2) The WC-Fe/Fe composite with SiC abrasive particles showed the highest wear resistance. The wear resistances of the WC-Fe/Fe composites were 38 and 96 times higher than those of gray cast iron under loads of 2 and 20 N, respectively. The main abrasive wear mechanism of the novel WC-Fe/Fe composite was protection of the matrix behind the WC bundles by the hard carbide.

- (3) The enhanced toughness of the WC-Fe/Fe composite is primarily attributed to two events. First, the G flakes disappeared from the Fe matrix because of the in situ reaction, which reduced the split action to the matrix. Second, crack initiation and propagation first occur in WC bundles because of their brittleness. When the crack propagates into the matrix, the crack propagation energy is absorbed by the matrix. The toughness of the composite was enhanced by inhibiting crack propagation.

## Acknowledgments

The project was supported by the National High Technology Research and Development Program of China (No. 2013AA031803) and the International S & T Cooperation Program of China (No. 2014DFR50630). The authors also acknowledge the financial support from the National Natural Science Foundation (No. 51374169), the Doctoral Scientific Research Foundation of Xi'an University of Technology (No. 101-451115013), and the Project of the Shaanxi Key Laboratory of Nano Materials and Technology (14JS046, 14JS048 and 13JS054).

## References

- J. Liu, J. Li, and C. Xu, Interaction of the Cutting Tools and the Ceramic-Reinforced Metal Matrix Composites During Micro-Machining: A Review, *CIRP J. Manuf. Sci. Technol.*, 2014, **7**, p 55–70
- L. Zhong, M. Hojamberdiev, F. Ye, H. Wu, and Y. Xu, Fabrication and Microstructure of In Situ Vanadium Carbide Ceramic Particulates-Reinforced Iron Matrix Composites, *Ceram. Int.*, 2013, **39**, p 731–736
- F. Velasco, R. Isabel, N. Antón, M.A. Martínez, and J.M. Torralba, High Speed Steel Composites: Sinterability and Properties, *Compos. A*, 2002, **33**(6), p 819–827
- S.K. Mishra, S. Biswas, and A. Satapathy, A Study on Processing, Characterization and Erosion Wear Behavior of Silicon Carbide Particle Filled ZA-27 Metal Matrix Composites, *Mater. Des.*, 2014, **55**, p 958–965
- A. Hauert, A. Rossoll, and A. Mortensen, Young's Modulus of Ceramic Particle Reinforced Aluminium: Measurement by the Impulse Excitation Technique and Confrontation with Analytical Models, *Compos. A*, 2009, **40**(4), p 524–529
- H.O. Pierson, *Handbook of Refractory Carbides and nitrides: Properties, Characteristics, Processing and Applications*, Noyes, Park Ridge, 1996
- Z. Li, Y. Jiang, R. Zhou, F. Gao, Q. Shan, and J. Tan, Thermal Fatigue Mechanism of WC Particles Reinforced Steel Substrate Surface Composite at Different Thermal Shock Temperatures, *J. Alloys Compd.*, 2014, **596**, p 48–54
- A. Liu, M. Guo, M. Zhao, and C. Wang, Microstructures and Wear Resistance of Large WC Particles Reinforced Surface Metal Matrix Composites Produced by Plasma Melt Injection, *Surf. Coat. Technol.*, 2007, **201**, p 7978–7982
- M. Zhao, A. Liu, M. Guo, D. Liu, Z. Wang, and C. Wang, WC Reinforced Surface Metal Matrix Composite Produced by Plasma Melt Injection, *Surf. Coat. Technol.*, 2006, **201**, p 1655–1659
- Z. Li, Y. Jiang, R. Zhou, D. Lu, and R. Zhou, Dry Three-Body Abrasive Wear Behavior of WC Reinforced Iron Matrix Surface Composites Produced by V-EPC Infiltration Casting Process, *Wear*, 2007, **262**, p 649–654
- J. Ji and J. Tang, Wear-Corrosion Behavior of Cast-In Composite Materials Reinforced by WC Particles, *Wear*, 1990, **138**, p 23–32
- K. Kambakas and P. Tsakirooulos, Solidification of High-Cr White Cast Iron–WC Particle Reinforced Composites, *Mater. Sci. Eng. A*, 2005, **413–414**, p 538–544
- S. Zhou, X. Dai, and H. Zheng, Microstructure and Wear Resistance of Fe-based WC Coating by Multi-track Overlapping Laser Induction Hybrid Rapid Cladding, *Opt. Laser Technol.*, 2012, **44**, p 190–197
- Z. Li, Y. Jiang, R. Zhou, Z. Chen, Q. Shan, and J. Tan, Effect of Cr Addition on the Microstructure and Abrasive Wear Resistance of WC-reinforced Iron Matrix Surface Composites, *J. Mater. Res.*, 2014, **29**, p 778–785
- Z. Li, Y. Jiang, R. Zhou, D. Lu, and R.F. Zhou, Dry Three-Body Abrasive Wear Behavior of WC Reinforced Iron Matrix Surface Composites Produced by V-EPC Infiltration Casting Process, *Wear*, 2007, **262**, p 649–654
- A. Liu, M. Guo, M. Zhao, and C. Wang, Microstructures and Wear Resistance of Large WC Particles Reinforced Surface Metal Matrix Composites Produced by Plasma Melt Injection, *Surf. Coat. Technol.*, 2007, **201**, p 7978–7982
- O.N. Çelik, Microstructure and Wear Properties of WC Particle Reinforced Composite Coating on Ti6Al4V Alloy Produced by the Plasma Transferred arc Method, *Appl. Surf. Sci.*, 2013, **274**, p 334–340
- Z. Chen, T. Zhou, P. Zhang, H. Zhang, W. Yang, H. Zhou, and L. Ren, Influences of Single Laser Tracks' Space on the Rolling Fatigue Contact of Gray Cast Iron, *Opt. Laser Technol.*, 2015, **72**, p 15–24
- M.T. Laugier, New Formula for Indentation Toughness in Ceramics, *J. Mater. Sci. Lett.*, 1987, **6**, p 355–356
- K. Aigner, W. Lengauer, and P. Ettmayer, Interactions in Iron-Based Cermet Systems, *J. Alloys Compd.*, 1997, **262–263**, p 486–491
- L. Niu, M. Hojamberdiev, and Y. Xu, Preparation of In Situ-Formed WC/Fe Composite on Gray Cast Iron Substrate by a Centrifugal Casting Process, *J. Mater. Process. Technol.*, 2010, **210**, p 1986–1990
- L. Niu, Y. Xu, and X. Wang, Fabrication of WC/Fe Composite Coating by Centrifugal Casting Plus In Situ Synthesis Techniques, *Surf. Coat. Technol.*, 2010, **205**, p 551–556
- B. Briscoe, *Wear of Polymers: An Essay on Fundamental Aspects*, *Tribol. Int.*, 1981, **14**(4), p 231–243
- E. Rabinowicz, *Friction and Wear of Materials*, Wiley, New York, 1965